www.sphinxsai.com

ChemTech

International Journal of ChemTech Research
CODEN (USA): IJCRGG ISSN : 0974-4290
Vol.6, No.5, pp 2834-2842, Aug-Sept 2014

N-N-methylene bis acrylamide: A novel fuel for combustion synthesis of zinc ferrite nanoparticles and studied by X-Ray photoelectron spectroscopy

R.Tholkappiyan[1]and K.Vishista[2]*

[1,2,]*Department of physics, Anna University, Chennai -25, India.

***Corres.author: vishista@yahoo.com**

\

Abstract: For the first time, N-N-methylene bi's acrylamide has been used as a novel fuel to synthesize the spinel type zinc ferrite nano particles by combustion method. X-Ray Diffraction (XRD) measurement confirms the formation of zinc ferrite with cubic structure. From FTIR analysis, the structure and the corresponding changes in the tetrahedral and octahedral bond stretching were investigated. The surface behavior of these nano particles was investigated by X-Ray Photoelectron Spectroscopy (XPS). The chemical elements and oxidation states of these nano particles were analyzed. The Photoelectron peaks of Zn 2p, Fe 2p, O 1s and C 1s with corresponding binding energy were observed. The morphology and porosity of the prepared ferrite samples was observed by scanning electron microscopy (SEM) analysis. The chemical elements and composition of the prepared nano particles were analyzed by Energy dispersive X-ray (EDX) technique. The optical behavior of these nanoparticles was characterized by UV-Diffuse reflectance studies (UV-DRS) and found to be 2.4 Ev.
Keywords: N-N-methylene bis acrylamide fuel**,** zinc ferrite, nano particle, combustion method, oxidation state, surface analysis.

1. Introduction

The magnetic materials of nanosize are much demand in power electronic devices, transformers and other magnetic storage circuits due to the rapid development in electronic technology. Many researchers are involved in magnetic materials especially in ferrite based materials. Various ferrite materials are available among them zinc ferrite is one of the high temperature stable material with cubic spinel ferrite structure in which zinc occupies tetrahedral site and iron occupy octahedral sites. Zinc ferrites are being studied and widely used in many applications such as hot-gas cleaning [1], photocatalytic properties [2], biomedicine as magnetically controlled transport of anti-cancer drugs treatment [3], magnetic cell separation [4], magnetic resonance imaging (MRI) [5] and heating mediators for cancer therapy [6] respectively. In recent reports, various synthesis methods like hydrothermal synthesis, microwave-assisted solvothermal method, Co-precipitation, sol-gel, low temperature, wet-milling process, mechanochemical reaction [7-12] etc. have been reported for nano crystalline $ZnFe_2O_4$ materials. Among them combustion method is simple and a huge yield of product of nano crystalline powders is obtained within a short span of reaction time. This combustion process, the amount of fuel to oxidizer ratio is important to form a pure phase compounds. According to concepts of propellant chemistry, the starting precursors like metal nitrate acts as an oxidizing agent where as corresponding fuels act as a reducing agent. Several fuels such as urea, citric acid ($C_6H_8O_7 \cdot 6H_2O$), glycine ($C_2H_5NO_2$) have been used for the synthesis of zinc ferrite nanoparticles. Here we choose N-N'-methylenebisacrylamide as fuel for preparing these zinc ferrite nanoparticles. On the other hand, N-N'-methylenebisacrylamide was used act as a crosslinker for the synthesis of thermosensitive porous hydrogels by radical polymerization method [13]. In this present work, we synthesized zinc ferrite nanoparticles with N, N'-methylenebisacrylamide as a fuel for the

first time by combustion method with a consistent amount of fuel-nitrate ratios. The structural properties of these zinc ferrite nano particles were characterized by X-Ray Diffraction (XRD). The structure and corresponding changes in the tetrahedral and octahedral bond stretching vibrations were studied by FT-IR analysis. To study the surface phenomenon and oxidation state these samples were characterized by X-Ray Photoelectron Spectroscopy (XPS). Detailed surface analysis of core level spectra of Zn 2p, Fe 2p, Ba 3d and O 1s peak were evaluated. The morphology and chemical compositions of the prepared ferrite samples was observed by scanning electron microscopy (SEM) and Energy dispersive X-ray (EDX) technique.

2. Experimental

2.1. Materials

Zinc nitrate hexahydrate purified ($Zn(NO_3)_2.6H_2O$) was bought from Merck, Iron (III) nitrate nonahydrate ($Fe(NO_3)_3.9H_2O$, 98-100% purity), N-N methylene bi's acrylamide ($C_7H_{10}N_2O_2$) and nitric acid were provided from Qualigens. All analytical reagents were used without further purification.

2.2. Preparation

Zinc ferrite nano particles were synthesized by combustion method using N-N methylene bi's acrylamide ($C_7H_{10}N_2O_2$) as fuel. Initially appropriate amounts of zinc nitrate ($Zn(NO_3)_2.6H_2O$) and iron nitrate ($Fe(NO_3)_3.9H_2O$) aqueous solution were prepared with addition of 20ml of distilled water. 10 ml of nitric acid (HNO_3) was added into the solution resulted in a clear aqueous solution. Stoichiometric amount of fuel (2.4183 g) was introduced into the mixture at the same time with stirring for 2 hr and then the mixture was heat treated at 80ºC for 40 min until the water evaporated. After that, it became a dark brown viscous gel. The obtained dark brown viscous gel was kept on a hot plate at 200ºC for 10 min an auto-ignition initiated to form a dried brown resin with the evolution of gaseous fumes. After complete reaction, a brownish zinc ferrite ash was produced. The actual time interval between the start of ignition and the end of the reaction was less than 20 s. Entire reaction process is illustrated in Fig. 1. Finally, as- prepared samples were kept out of hot plate and ground using an agate motor and pestle to form fine powders.

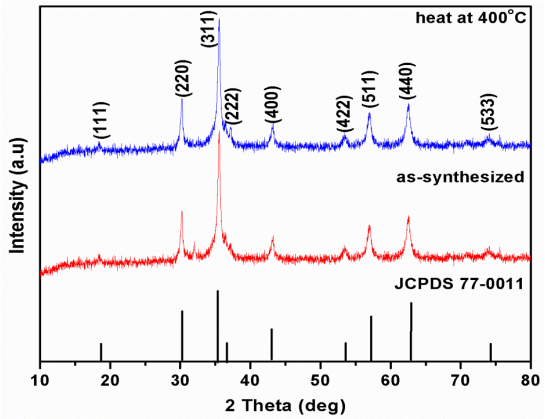

Fig. 1 X-ray diffraction patterns of the synthesized $ZnFe_2O_4$ powders by combustion method using N-N methylene bias acrilamide as fuel.

2.3. Characterization

The crystal structure of the as-synthesized powder was identified by X-ray measurements of Bruker D2 Phaser Powder X-ray diffractometer using CuKα radiation (λ = 1.5418 Å) in the range of 10º to 80º with step mode of 0.2/min. FT-IR studies of prepared samples were investigated in the wave number region 4000-400 cm^{-1} at room temperature using BRUKER ALPHA spectrometer with opus 6.5 (version) software by KBr pellet method. Information about the oxidation states of these samples was obtained from X-Ray Photoelectron Spectroscopy (XPS) using Kratos Analytical Axis Ultra DLD with Al Kα1 source. The energy of an X-ray photon of 1.486 keV with pass energy of 160 eV was used for the survey spectrum and 40 eV for narrow scans. The angle between the normal to the sample surface and the direction of photoelectron collection are perpendicular to each other. The spectra were collected using the combination of electrostatic and magnetic lens (hybrid mode) for an analyzed area of (700x300 µm). Surface charging effects were minimized using a charge balance operating at 3.6 V and 1.8 V maintained as filament bias. The surface morphology was analyzed using

scanning electron microscope (SEM with EDX) JSM-6360 LA (JEOL, Japan (JEOL) with an accelerating voltage of 15 kV. The optical behaviour of the investigated powder samples were performed by UV-2102 PCS Spectrophotometer.

3. Results and discussion

Effect of fuel type on the auto combustion synthesis of $ZnFe_2O_4$

Synthesis of simple and complex oxide materials by the combustion of redox compounds is simple, fast, attractive for energetically economic and produce high yield purity products compared to the conventional methods. In this regard, a novel fuel N-N methylene bis acrylamide ($C_7H_{10}N_2O_2$) was used to synthesis $ZnFe_2O_4$ nano particles by combustion method. The fuel-nitrates combustion process, the exothermic redox reaction can be expressed as given below,

$$Zn\ (NO_3)_2.6H_2O + 2\ Fe\ (NO_3)_3.9H_2O + 1.17647C_7H_{10}N_2O_2 \longrightarrow ZnFe_2O_4 + 5.17647N_2 \uparrow + 8.23529CO_2 \uparrow + 5.88235H_2O\uparrow$$

In the above reaction, the N_2, CO_2 and H_2O are evolved as the gaseous products. The total reducing valence of N-N methylene bis acrylamide ($C_7H_{10}N_2O_2$) is +34 and the total valance of nitrates is -40. The stoichiometric composition of the fuel–nitrate mixture becomes 2× (-15) +1× (-10) +n (+34) = 0, n=1. 17647 mol in the reaction.

Here, fuel-nitrates composition indicates fuel/NO_3^-=0.78431 (fuel-to-nitrate ion ratio). In this present work, we consider the stoichiometric amount of fuel to nitrate composition is 0.78431 and results in the formation of pure nano-size zinc ferrite.

3.1. X-ray diffraction studies

The phase purity and structure of the sample were analyzed by X-ray diffraction. Fig. 1 shows the X-ray diffraction (XRD) pattern of as prepared zinc ferrite nano particles. It shows that all the diffraction peaks were indexed to the crystal plane of (111), (220), (311), (222), (400), (422), (511), (440) and (533) in the XRD pattern and are well fitted. No other extra/impurity diffraction peaks were detected. It is clear that these peaks can be attributed to the spinel type cubic structure (JCPDS no. 077-0011). The broad diffraction peak indicates that the prepared sample is in the order of nano size. In order to determine the average crystallite size (d) of the as-synthesized powder Scherrer formula was used and calculated by an equation [14],

$$d = 0.9\ \lambda/(\ \beta\cos\ \theta) \qquad (1)$$

where d is the average crystallite size, θ is the diffraction angle, λ(0.154 nm) is the wave length of X-ray beam, (FWHM). The average crystallite (d) size of the pure zinc ferrite is 23.9 nm and listed in Table 1. The lattice constant (a) for the prepared zinc ferrite was calculated using the equation [14],

$$a= [d^2 /(h^2+k^2 +l^2)]^{1/2} \qquad (2)$$

Where d is the value of d-spacing of line in XRD pattern and (hkl) are the Miller indices. From the Table 1 calculated values of lattice constant of the prepared zinc ferrite sample was 8.373 Å with accuracy of ± 0.002 Å. The X-ray density 'd_X' of the zinc ferrite was calculated using the following expression [14].

$$d_X=8M/NV \qquad (3)$$

Where M is the molecular weight of the sample, N is the Avogadro's number=$6.023x10^{23}$ and V is the volume unit cell. The value of X-ray density of prepared nano particle was 5.45 g/cm^3 and mentioned in Table 1. The specific surface area (S) was determined from the X-ray density of the sample (d_X) and diameter of the particle (D) using the following equation [14].

$$S=6/d_XD \qquad (4)$$

The values of specific surface area of zinc ferrite nano particles was 45.94 m^2/g are listed in **Table 1.**

The elastic strain (E) of the samples was calculated using the formula [15],

$$E = \beta / 2 \cot \theta \quad (5)$$

Where β is the full-with half maximum, θ is the diffraction angle. The elastic strain for the prepared zinc ferrite was found to be 0.0973.

Table 1: Structural parameters obtained from X-ray diffraction studies.

Sample	Fuel (g)	Average Crystallite size (nm)	X-Ray Density(d_x) g/cm^3	Lattice Constant (Å)	Surface Area(m^2/g)	Elastic Strain (E)
$ZnFe_2O_4$	2.4183	23.93	5.45	8.373	45.947	0.0973

3.2. FT-IR characterization

IR spectroscopy is an one of the important tool to get information about the cationic distribution in the spinel structure through the crystal's vibrational modes. Fig. 2 shows the infrared spectrum of the zinc ferrite at room temperature in the frequency range of 400–4000 cm^{-1}. It is known that spinel type zinc ferrite is the normal cubic structure in which Zn^{2+} ion occupies tetrahedral (A) site and Fe^{3+} ion occupy octahedral (B) sites. For the investigated zinc ferrite two strong absorption bands namely high frequency band (ν_1) and low frequency band (ν_2) were observed in the FT-IR spectra. The high frequency band (ν_1) that was observed at around 549.5 cm^{-1} is attributed to metal–O bond stretching vibration in tetrahedral site. Low frequency band (ν_2) at ~434 cm^{-1} is assigned to metal–O bond stretching vibration in the octahedral (B) site of the zinc ferrite. These two observed bands ν_1 and ν_2 difference is attributed to the difference in the Fe^{3+}–O^{2-} distance for tetrahedral and octahedral complexes [16]. These difference in the vibrational frequency is also due to bond length (A-O), bonding force and the cation mass [17]. The absorption band at 1380.7 cm^{-1} is identified as stretching vibration of anti-symmetric NO_3^-. This NO_3^- ions occurs during combustion process with the evolution of gaseous fumes. Hence, the combustion process can be considered as a exothermic redox reaction between the metal nitrates (oxidizing agents) and an appropriate fuel as reducing agent [18].

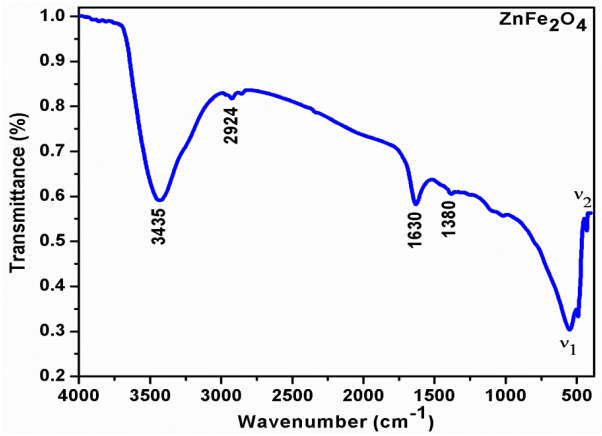

Fig. 2 Infrared spectra of zinc ferrite nano particles at room temperature.

3.3. X-Ray photoelectron spectroscopy studies

Surface analysis and chemical states of the prepared sample were investigated by X-Ray photoelectron spectroscopy (XPS). Fig. 3 shows XPS wide spectrum of zinc ferrite nano particles prepared by combustion method. The photoelectron peaks of Zn 2p, Fe 2p and O 1s along with C 1s were observed in this spectrum. The C 1s (carbon) peak present in this sample is due to the carbon formed during the synthesis of zinc ferrite by combustion process. The data of atomic ratio for zinc ferrite nano particles are mentioned in Table 2. From this table the ratio of Zn/Fe/O in the sample is nearly close to 1/2/4 agreeing with the expected chemical formula of $ZnFe_2O_4$. For detailed analysis of this wide spectrum CASA XPS Version 2.3 software package was used to fit the individual peak spectra of Zn 2p, Fe 2p, O1s and C1s by Shirley type of background was subtracted.

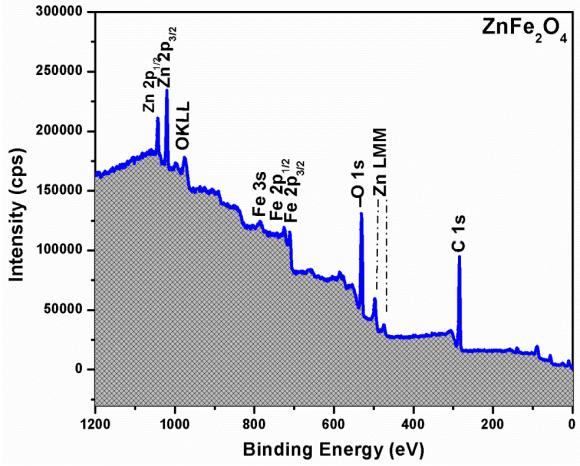

Fig. 3 Survey spectrum of zinc ferrite nano particles.

Table 2: Wide spectrum peaks parameter of zinc ferrite nano particles obtained from XPS data.

Name	Position (eV)	FWHM (eV)	At%
Zn 2p	1020	3.644	1.63
Fe 2p	710	4.757	1.92
O 1s	531	4.708	27.41
C 1s	284	3.6	69.04

Fig. 4a (insert) shows the XPS spectra of Zn 2p peak. The two major peaks of Zn $2p_{3/2}$ and Zn $2p_{1/2}$ were present in this spectra with binding energy values of 1021.1 eV and 1043.3 eV [19]. Fig. 5a shows the Zn 2p peak deconvolution spectra of zinc ferrite nano particles. It exhibits two sub-peaks. The peak at 1020.4 eV and 1022.2 eV for Zn $2p_{3/2}$ indicates the presence of Zn^{2+} ion in the zinc ferrite nano particles. This is similar to the result reported by *Y. Y. Tay, S. Li et.al,* for nanocrystalline ZnO whose binding energy of Zn $2p_{3/2}$ is located at 1022.0 eV [20]. The other two sub-peaks at 1042.03 and 1044.07 eV correspond to intensity peak of Zn $2p_{1/2}$.

Fig. 4b (insert) shows the Fe 2p core shell XPS spectra of zinc ferrite. It consists of two features of binding energy values observed at 711.21 eV for Fe $2p_{3/2}$ and 725.81 eV for Fe $2p_{1/2}$ respectively, with a satellite peak at 718.2 eV. This result is in close agreement with previous literature for Fe^{3+} ion in ferrite materials [21-22]. Significantly, the deconvolution spectra of Fe 2p shown in Fig. 2 can be fitted into four distinct peaks located at 709.3 eV, 713.43 eV, 723.88 eV and 729.73 eV. These peaks correspond to the binding energies of Fe $2p_{3/2}$-Fe^{2+}, Fe $2p_{3/2}$-Fe^{3+}, Fe $2p_{1/2}$-Fe^{2+} and Fe $2p_{3/2}$-Fe^{3+} ions [23-24]. Therefore, the oxidation states of iron (Fe) in the prepared nano particles definitely consists of both Fe^{3+} and Fe^{2+} ions. According to Wen's report [25], the spinel system (AB_2O_4) Fe^{2+} occupies B sites at 709.5 eV where as Fe^{3+} occupies both A and B sites with binding energies at 710.6 and 711.3 eV respectively.

The XPS spectrum of the O 1s region was detected at 530.23 eV, as shown in Fig. 4c (insert). Specifically, O 1s region in Fig. 5c can be deconvoluted into five distinct peaks at 528.31 eV, 529.67 eV, 530.54 eV, 531.61 eV and 532.63 eV respectively. These peaks are associated with corresponding binding energies of O^{2-}, OH^-, H_2O, C-O-metal and C=O groups observed on the surface of the sample [26-27].

The C 1s core-level XPS spectra as shown in Fig. 4d. It shows two components at 283.9 eV and 286.4 eV. The peak at 283.9 eV can be attributed to C-H bond. The signal at 286.4 eV can be assigned to C-O bond respectively [28-29].

3.4. SEM and EDX analysis

Fig. 5(a-c) shows the SEM images of prepared zinc ferrite nano particles with different magnifications. It shows that nano particles are agglomerated with porous network. During the combustion process, large amount of gases evolved when the reaction reached the critical temperature; leading to the formation of pores in the prepared nano particles. The compositional and confirm the presence of the nanocrystalline zinc ferrites prepared by combustion process were carried out by energy dispersive X-ray analysis (EDX). Fig. 5d shows the

EDX spectra of zinc ferrite nano particles. The presence of Zn, Fe and O elements is confirmed form the EDX spectra. No other elements or impurity was detected. This confirms the purity of the prepared nano particles. This is further supported by XRD and XPS analysis. The observed atomic% and weight % of Zn and Fe is tabulated in insert of Fig. 5d. These values are well matched with expected atomic ratio of Zn:Fe:O spinel type nano particles prepared by combustion method. Hence, this method is completely favorable for formation of pure zinc ferrite nano particles.

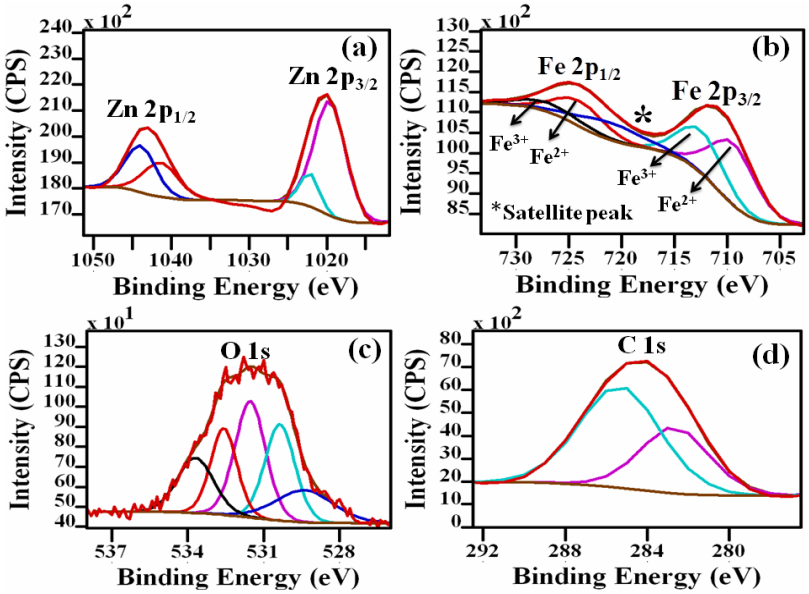

Fig. 4 Deconvolution XPS spectra of (a) Zn 2p, (b) Fe 2p, (c) O 1s and (d) C 1s of zinc ferrite nano particles.

Table 3: Deconvolution parameters of zinc ferrite nano particles from Zn 2p, Fe 2p and O 1s peak from XPS.

Sample	Peak[x]	Position	Percent (%)[y]	FWHM[z]
$ZnFe_2O_4$	Zn $2p_{3/2}$	1019.12	43.11	2.08
	Zn $2p_{3/2}$	1020.41	15.56	3.12
	Zn $2p_{1/2}$	1043.27	31.05	2.47
	Zn $2p_{1/2}$	1043.03	10.28	3.61
	Fe $2p_{3/2}$- Fe^{3+}	710.40	57.59	1.27
	Fe $2p_{3/2}$- Fe^{2+}	717.43	11.02	3.11
	Fe $2p_{1/2}$ -Fe^{3+}	723.88	27.74	2.95
	Fe $2p_{1/2}$- Fe^{2+}	729.73	3.65	3.54
	lattice O^{2-}	528.31	4.57	1.17
	OH^-	529.67	11.61	1.27
	H_2O	530.54	23.71	1.27
	C-O-metal	531.61	27.59	1.35
	C=O	532.63	18.34	1.22

[x]represents the Zn 2p, Fe 2p spectra with corresponding peak positions of Zn $2p_{3/2}$, Zn $2p_{1/2}$, Fe $2p_{3/2}$, Fe $2p_{1/2}$ and oxygen surface species: lattice O^{2-}: oxygen bonded to metal; OH^- group: hydroxyl bonded to metal; H-O-H: absorbed water; C-O-metal group: C-O- bonded to metal and C=O group. [y]percentage that contribution of each peak to the total number of counts in Zn 2p, Fe 2p, O 1s peak. [z]Full Width Half Maximum of each peak in the Zn 2p, Fe 2p, O 1s Spectra.

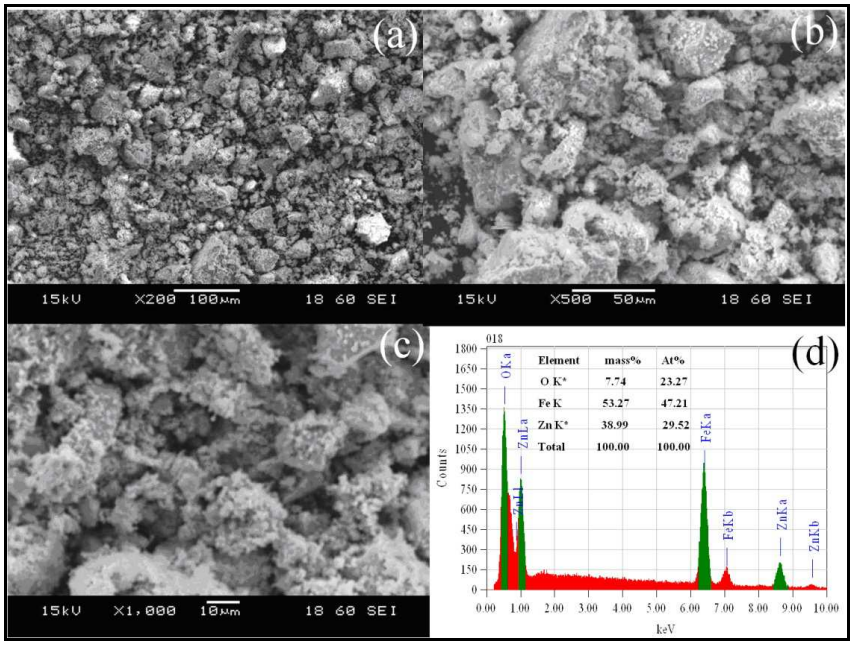

Fig. 5 (a-c) SEM micrographs with different magnifications of $ZnFe_2O_4$ nano particles (d) EDX pattern of $ZnFe_2O_4$ nano particles.

3.5. UV- DRS studies

The optical properties of zinc ferrite nanoparticles are illustrated by UV-vis diffuse reflection measurement. Fig. 6 shows the diffuse absorption spectra of prepared zinc ferrite nanoparticles. From the absorption spectra pure zinc ferrite nanoparticles are observed in the UV- Visible region of 200–500 nm and can find potential application as optical devices.

The optical absorption coefficient can be calculated from the reflectance data by using Kubelka-Munk function [30],

$$\alpha = (1-R)^2/2R \qquad (6)$$

where R is the diffuse reflectance.

The optical band gap of zinc ferrite nanoparticles is determined using the Tauc relation.

$$(\alpha h\nu) = A\,(h\nu - Eg)^n \qquad (7)$$

Where α is the absorption coefficient, A is the constant, Eg is the energy gap, hν is the energy of the incident photon, and n is an index that characterizes the optical absorption process [1].

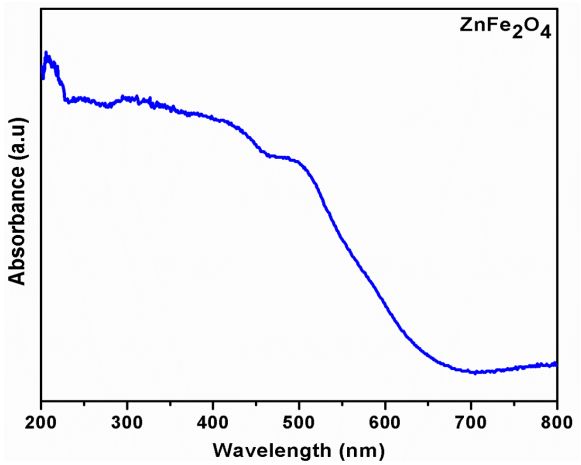

Fig. 6 UV-Vis absorbance spectra of zinc ferrite nanoparticles.

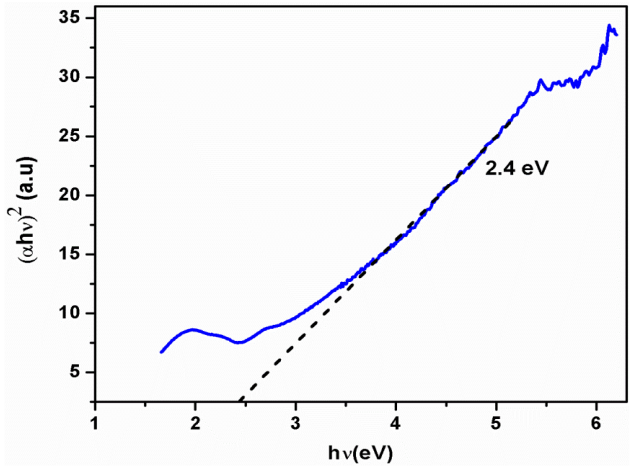

Fig. 7 Tauc polts of $(\alpha h\nu)^2$ against hν(eV) for zinc ferrite nano powders.

Fig. 7 shows the Tauc polts of $(\alpha h\nu)^2$ against hν(eV) of zinc ferrite nano powders. The band gap energy was found to be 2.4 eV which is in good agreement with previously reported values [39]. This band gap value is quiet close to the optimum band gap required for optical applications as photo catalysts [31].

4. Conclusions

Pure zinc ferrite nano particles were prepared by combustion method using novel type of fuel (N-N methylene bi's acrylamide). The structural properties of these zinc ferrite nano particles were characterized by X-Ray Diffraction (XRD). It confirms the formation of cubic spinel type zinc ferrite nano particles with average crystallite size of 23.93 nm. No other extra/ impurity phase were observed. The formation of structure and corresponding changes in the bond stretching vibration of tetrahedral and octahedral metal complexes were investigated by FTIR. The surface phenomenon and oxidation state these samples were characterized by X-Ray Photoelectron Spectroscopy (XPS). Detailed surface analysis of core level spectra of Zn 2p, Fe 2p, Ba 3d and O 1s peak were studied and found to be 2+ state for zinc and 3+ states for iron on the surface of prepared sample. The porosity/voids and morphology of the prepared ferrite nano particles were observed from SEM analysis. To confirm the presence of chemical elements and composition of the prepared nano particles, EDX was used. From the UV-DRS studies, the optical band gap was found to be 2.4 eV.

References

[1] Toshimitsu Suzuki, Na-oki Ikenaga, Hiro-aki Matsushima, and Yousuke Ohgaito, preparation of zinc ferrite in the presence of carbon material and its application to hot-gas cleaning, Fuel Chemistry Division Preprints, 2003, 48(1), 415.

[2] S.W. Caoa, Y.J. Zhua, G.F. Cheng and Y.H. Huang, "$ZnFe_2O_4$ nanoparticles: microwave-hydrothermal ionic liquid synthesis and photocatalytic property over phenol", J. Hazard. Mater., [171], 1-3, (2009), 431–435.

[3] Z.H. Zhou, J.M. Xue, J. Wang, H.S.O. Chan, T. Yu, Z.X. Shen, $NiFe_2O_4$ nanoparticles formed in situ in silica matrix by mechanical activation, J. Appl. Phys 2002, 91, 6015.

[4] G. Zhang, L. Chunsheng, C. Fangyi, J. Chen, $ZnFe_2O_4$ tubes: Synthesis and application to gas sensors with high sensitivity and low-energy consumption, Sensors & Actuators B. 2007, 120, 403-410.

[5] Kondo, A., Kamura, H., Higashitani, K., Development and application of thermosensitive magnetic immunomicrospheres for antibody purification, Appl. Microbiol. Biotechnol., (1994) 41, pp. 99-105.

[6] Safarik, I., Safarikova, M., Use of magnetic techniques for isolation of cells (1999) J. Chromatogr. B Biomed. Sci. Appl., 722, pp. 33-53.

[7] Shu-Hong Yu, Takahiro Fujino, Masahiro Yoshimura, Hydrothermal synthesis of ZnFe2O4 ultrafine particles with high magnetization, Journal of Magnetism and Magnetic Materials 2003, 256, 420–424.

[8] Qiaoling Li, Changchuan Bo, Wenting Wang, preparation and magnetic properties of $ZnFe_2O_4$ nanofibers by coprecipitation-air oxidation method, Materials Chemistry and Physics 2010, 124, 891.

[9]. Aurelija Gatelytė, Darius Jasaitis, Aldona Beganskienė, Aivaras Kareiva, Sol-Gel synthesis and Characterization of selected transition metal nano-ferrites, Materials Science 2011, 17(3), 1392–1320.
[10] Xinyong Li, Gongxuan Lu, Shuben Li, synthesis and Characterization of fine particle ZnFe2O4 powders by a low temperature method, Journal of Alloys and Compounds 1996, 235, 150-155.
[11] Sadan Ozcan, Burak Kaynar, Musa Mutlu Can, Tezer Fırat, Synthesis of ZnFe2O4 from metallic zinc and iron by wet-milling process, Materials Science and Engineering B 2005, 121, 278–281.
[12] Huaming Yang, Xiangchao Zhang, Chenghuan Huang, Wuguo Yang, Guanzhou Qiu, Synthesis of ZnFe2O4 nanocrystallites by mechanochemical reaction, Journal of Physics and Chemistry of Solids 2004, 65, 1329–1332.
[13] Takehiko Gotoh, Yuko Nakatani, Shuji Sakohara, Novel Synthesis of Thermosensitive Porous Hydrogels, Journal of Applied Polymer Science, 69 (1988) 895.
[14] S.J. Haralkar, R.H.Kadam, S.S More, Sagar E.Shirsath, M.L.Mane, SwatiPatil, D.R.Mane," Substitutional effect of Cr3þ ions on the properties of Mg–Zn ferritenanoparticles", Physica B 407 (2012) 4338–4346.
[15] A. Nirmalesh Naveen, Subramanian Selladurai, investigation on physiochemical properties of Mn Substituted spinel cobalt oxide for supercapacitor Applications, Electrochimica Acta 125 (2014) 404–414.
[16] B.K. Labde, Madan C. Sable, N.R. Shamkwar, Mater. Lett. 57 (2003) 1651.
[17] S.A. Patil, V.C. Mahajan, A.K. Ghatage, S.D. Lotke, Mater. Chem. Phys. 57 (1998) 86.
[18] R. Tholkappiyan, K. Vishista. Advanced Science, Engineering and Medicine. 6 (2014) 311-317.
[19] Pan Feng, Guo Ying, Cheng Feng-Feng, Fa Tao and Yao Shu-De, Synthesis of ZnFe2O4 nanomagnets by Fe-ion implantation into ZnO and post-annealing, Chin. Phys. B Vol. 20, No. 12 (2011) 127501.
[20] Y. Y. Tay, S. Li, C. Q. Sun and P. Chen, Size dependence of Zn $2p_{3/2}$ binding energy in nanocrystalline ZnO, Applied Physics Letters 88, 173118(2006).
[21] C. Barcena, A.K. Sra, G.S. Chaubey, C. Khemtong, J.P. Liu, J. Gao, Chem. Commun. (2008) 2224–2226.
[22] Y. Hou, X.Y. Li, Q.D. Zhao, X. Quan, G.H. Chen, Adv. Funct. Mater. 20 (2010) 2165–2174.
[23] J.F. Moulder, J. Chastain, Handbook of X-ray Photoelectron Spectroscopy: A Reference Book of Standard Spectra for Identification and Interpretation of XPS Data, Physical, Electronics, 1995.
[24] M. Wuhn, Y. Joseph, P.S. Bagus, A. Niklewski, R. Puttner, S. Reiss, W. Weiss, M. Martins, G. Kaindl, C. Woll, J. Phys. Chem. B 104 (2000) 7694–7701.
[25] Chen, M.; Wang, X.; Yu, Y. H.; Pei, Z. L.; Bai, X. D.; Sun, C.; Huang, R. F.; Wen, L. S. Appl. Surf. Sci. 2000,158, 134-140.
[26] J.F. Marco, J.R. Gancedo, M. Gracia, J.L. Gautier, E.I. Rios, J. Solid State Chem. 153 (2000) 74–81.
[27] A.C. Tavares, M.I. da Silva Pereira, M.H. Mendonça, M.R. Nunes, F.M. Costa, C.M. Sá, J. Electroanal. Chem. 449 (1998) 91–100.
[28] P. J. Tarcha, L. Salvati, R. W. Johnson, Surf. Sci. Spectra 2001, 8, 312 – 316.
[29] M. V squez, G. J. Cruz, M. G. Olayo, T. Timoshina, J. Morales, R. Olayo, Polymer 2006, 47, 7864 – 7870.
[30] J.S. Jang, S.J. Hong, J.S. Lee, J. Korean Phys. Soc. 54 (1) (2009) 204.
[31] Pramod H. Borse, J. Korean Phys. Soc. 59 (4) (2010) 2750.

*****